RESEARCH PAPER

Pinch-off mechanism for Taylor bubble formation in a microfluidic flow-focusing device

Yutao Lu · Taotao Fu · Chunying Zhu · Youguang Ma · Huai Z. Li

Abstract The present work aims at studying the nonlinear breakup mechanism for Taylor bubble formation in a microfluidic flow-focusing device by using a high-speed digital camera. Experiments were carried out in a square microchannel with cross section of 600×600 μm. During the nonlinear collapse process, the variation of the minimum radius of bubble neck (r_0) with the remaining time until pinch-off (τ) can be scaled by a power–law relationship: $r_0 \propto \tau^\alpha$. Due to the interface rearrangement around the neck, the nonlinear collapse process can be divided into two distinct stages: liquid squeezing collapse stage and free pinch-off stage. In the liquid squeezing collapse stage, the neck collapses under the constriction of the liquid flow and the exponent α approaches to 0.33 with the increase in the liquid flow rate Q_l. In the free pinch-off stage, the value of α is close to the theoretical value of 0.50 derived from the Rayleigh–Plesset equation and is independent of Q_l.

Keywords Microfluidics · Multiphase flow · Nonlinear dynamics · Interface · Confinement · Pinch-off

List of symbols

p	Capillary pressure, Pa
Q_l	Liquid volumetric flow rate, mL h^{-1}
Q_g	Gas volumetric flow rate, mL h^{-1}
Q_F	Liquid volumetric flow rate through the flow-focusing region, mL h^{-1}
Q_N	Liquid volumetric flow rate calculated from the pictures, mL h^{-1}
r	Radius of the bubble neck, μm
r_0	Minimum radial radius of the neck, μm
r_c	Minimum axial radius of the neck, μm
t	Neck collapse time, μs
t_c	Moment of bubble pinch-off, μs
t_{cap}	Capillary time, μs
V_N	Volume of the neck, mL
w_b	Width of the bubble neck, μm
w_d	Depth of the channel, μm

Greek letters

α	Exponent for radial curvature
β	Exponent for axial curvature
λ	Slenderness of the neck (r_c/r_0)
η	Viscosity, m Pa s
ρ	Density, kg m^{-3}
σ	Surface tension, m N m^{-1}
τ	Remaining time to pinch-off, μs

Dimensionless groups

Ca	Capillary number ($u\eta_l/\sigma$)
Re	Reynold number ($\rho_l r_0 r_0'/\eta_l$)
We	Weber number ($\rho r_0 (r_0')^2/\sigma$)

Subscripts

c	Critical time for bubble pinch-off
cap	Capillary time
F	Flow-focusing region

Y. Lu · T. Fu (✉) · C. Zhu · Y. Ma (✉)
State Key Laboratory of Chemical Engineering,
School of Chemical Engineering and Technology,
Tianjin University, Tianjin 300072, China
e-mail: ttfu@tju.edu.cn

Y. Ma
e-mail: ygma@tju.edu.cn

H. Z. Li
Laboratory of Reactions and Process Engineering,
University of Lorraine, CNRS, 1, rue Grandville,
BP 20451, 54001 Nancy Cedex, France

g   Gas
kfps   Kilo frames per second
l   Liquid
N   Neck of the bubble

1 Introduction

In recent years, microfluidic technology has been widely applied in chemical engineering, biological engineering, medical engineering, food engineering, analytical chemistry and materials synthesis, etc., owing to its excellent performances of heat and mass transfer and monodispersion (Ferrara et al. 2009; Hartman et al. 2010; Kashid et al. 2011; Nghe et al. 2011; Tadmor et al. 2011; Tumarkin et al. 2011; Utada et al. 2005; Wang et al. 2010; Wörner 2012; Zhao et al. 2007). In these applications, the Taylor flow, characterized by the alternate gas and liquid slugs, is often encountered in fast multiphase reactions and analytical chemistry, due to its broad operation range and negligible back mixing (Abadie et al. 2012; Kreutzer et al. 2005; Li et al. 2011; Sun and Cubaud 2011). In the application of Taylor flow, the formation and breakup process of bubbles is crucial to regulate the size, polydispersity of the products (Ganan-Calvo and Gordillo 2001; Garstecki et al. 2004; Garstecki et al. 2005). Therefore, it is of great significance to systematically study the formation and breakup mechanism for the Taylor bubble in microchannels.

Compared with bubbles formed in large-scale devices, the breakup of gaseous thread for bubbles formed in microchannels exhibits several special characteristics owing to the confinement of the interface by the channel wall and the liquids flowing around the gaseous thread (Dollet et al. 2008; Fu et al. 2012a, b; Garstecki et al. 2005; van Hoeve et al. 2011; van Steijn et al. 2009). For example, the geometrical confinement could suppress the capillary instability, resulting in the linear collapse of the gaseous thread with time (Garstecki et al. 2005). Garstecki et al. (2005) originally investigated the effects of confinement on bubble formation in a flow-focusing device and observed two stages for the thinning of the gaseous neck: linear collapse and nonlinear breakup. For the linear collapse stage, the collapse speed was proportional to the liquid flow rate due to the geometrical confinement of the microchannel. Once the interface detached from the wall, the nonlinear collapse began, and the neck collapse speeded up immediately resulting from the Rayleigh-Plateau instability. Furthermore, Dollet et al. (2008) confirmed the argument by studying the effect of channel geometry on the breakup of gaseous thread and found that the relationship between the minimum width r_0 of the gaseous thread and the remaining time τ until the pinch-off during the nonlinear collapse of bubbles could be scaled by a power–law of $r_0 \propto \tau^{1/3}$. This argument was also identified for bubbles formed in a completely confined flow-focusing microchannel by Fu et al. (2010).

Regarding the effects of the liquid flowing around the gaseous thread on the nonlinear collapse for bubble formation, van Steijn et al. (2009) observed the reverse flow in the gutters between the channel wall and the gaseous thread for bubbles formed in a T-junction and argued that the reverse flow initiated the nonlinear collapse of the gaseous thread. van Hoeve et al. (2011) recently found that the flow around the gaseous thread affected the scale of the exponent: when τ was larger than τ_{cap} (τ_{cap} represents the capillary time), the collapse process could be scaled as $r_0 \propto \tau^{1/3}$; however, when τ was less than τ_{cap}, $r_0 \propto \tau^{2/5}$. It could be obviously concluded from the above-mentioned analyses that the nonlinear pinch-off dynamics for bubbles formed in microfluidic devices remains in debate up to now, such as the role of the liquid around the gaseous thread, the collapse laws and the dominating forces exerted on the interface for the pinch-off dynamics for bubble formation.

Although several efforts have been devoted to bubble formation in microfluidic devices, however, the pinch-off mechanism for Taylor bubble formation in such devices has not been fully understood. This work aims at throwing new insights into the nonlinear breakup mechanism for Taylor bubble formation in a flow-focusing device. And the effects of liquid constriction, liquid viscosity and surface tension on the nonlinear collapse process for bubble formation are also studied.

2 Experimental procedures

To ensure the axisymmetry of the gaseous neck and obtain enough duration of nonlinear collapse, a square cross-sectional microchannel of 600×600 μm was adopted (Dollet et al. 2008; van Hoeve et al. 2011). The channel was fabricated in a polymethyl methacrylate (PMMA) - plate by precision milling and then sealed with another PMMA plate by screws. Stainless steel tubes ($d_i = 1$ mm) were used to connect the inlets and outlet of the microchannel to tygon tubes (ID = 1.02 mm), which were employed to transport fluids from the supplies to the microchannel. The gas and liquid flow rates were controlled separately by syringe pumps (PHD 2000, Harvard Apparatus, America).

The dispersed phase was infused to the main channel, and the continuous phase to the two lateral channels
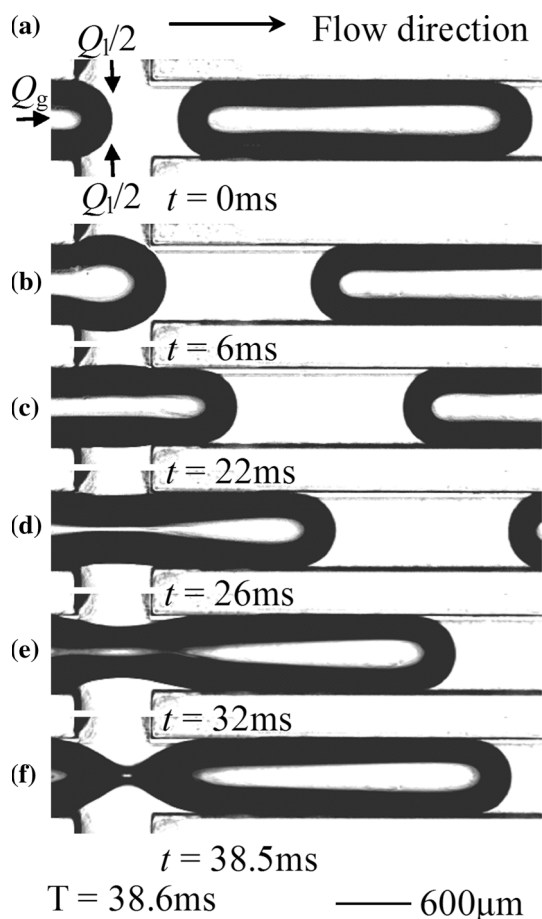
Fig. 1 Dynamics of Taylor bubble formation in turpentine oil. The moment of neck breakup is defined as $t = 0$ ms. $Q_l = Q_g = 30$ mL h^{-1}

Table 1 Physical properties of various continuous phases

Solution (wt)	Density	Viscosity	Surface tension	Contact angle
	ρ (kg m^{-3})	μ (m Pa s)	σ (m N m^{-1})	θ (°)
Turpentine oil	867.0	1.30	24.0	<30
Ethanol	774.6	1.14	22.6	<30
60 % Ethanol/water	885.8	2.06	27.9	<30
30 % Ethanol/water	951.1	2.04	33.9	45
20 % Ethanol/water	967.3	1.70	40.0	58
10 % Ethanol/water	981.6	1.33	50.1	65
5 % Ethanol/water	989.9	1.17	57.7	72
55 % Glycerol/ethanol	1,010.0	13.4	27.8	<30
50 % Glycerol/ethanol	984.7	9.85	25.6	<30
40 % Glycerol/ethanol	940.4	5.35	23.5	<30
30 % Glycerol/ethanol	899.9	3.28	24.2	<30
20 % Glycerol/ethanol	857.1	2.18	24.0	<30

(Fig. 1a). As the fluids converging, the Taylor bubble was formed in the flow-focusing region. It took at least 300 s to ensure that the flow was steady after a new flow condition was set. The scene of bubble formation was magnified by a microscope (ECLIPSE Ti-U, Nikon, Japan) then recorded by a high-speed digital camera (MotionPro Y5, IDT, USA). The highest frequency of the camera was 100 kfps (kilo frame per second), with a shortest exposure time of 1 μs. To more clearly visualize and record the evolution of the bubble formation and breakup, 50 and 4 kfps were chosen separately for different experimental conditions. The spatial resolution of the images was up to 1.5 μm pixel^{-1}.

Nitrogen and turpentine oil were used as the dispersed and the continuous phases, respectively. Then, a series of solutions of glycerol in ethanol and ethanol in deionized water were used as the continuous phase to investigate the influence of the viscosity and the surface tension on the breakup, respectively. The detailed physical properties for the continuous phases were listed in Table 1.

3 Result and discussion

3.1 The nonlinear collapse characteristic for Taylor bubble formation

A typical bubble formation sequence is shown in Fig. 1. At the beginning, the gaseous thread expands in the flow-focusing region (Fig. 1a, b) (Fu et al. 2010). When the gaseous thread tip blocks the main channel, the convex neck collapses linearly with time under liquid squeezing (Fig. 1c) (Garstecki et al. 2005). And when the width of the neck of the gaseous thread is less than the width of the channel, a concave neck is formed under the liquid constriction with the gaseous thread completely blocking the main channel and then the nonlinear collapse begins (Fig. 1d–f) (Dollet et al. 2008).

The photographic sequences are analyzed by using a home-made Matlab program. The contour of the neck is extracted from the images using intensity thresholding and linear interpolation between pixels to achieve subpixel accuracy. Then, a polynomial function, $r = f(z)$ is obtained to describe the neck contour using numerical fitting method. As shown in Fig. 2, the white curve is the result of seventh-order polynomial fitting, which totally overlaps the profile of the neck. It is identified that the fitting results
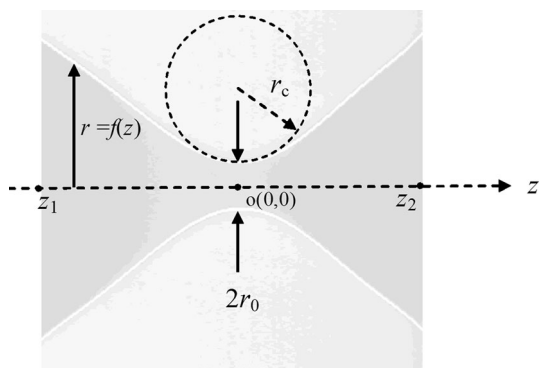
Fig. 2 Interfacial contour and geometrical parameters of the axisymmetric gaseous neck before the pinch-off. The *white curve* is used to describe the profile of the neck

could be used to describe the gas–liquid interface precisely. Garstecki et al. (2005) reported the neck was axisymmetric during nonlinear collapse by simulation and the argument was confirmed by van Steijn et al. (2009) and van Hoeve et al. (2011). Based on the consensus of the axisymmetric neck, we set up a cylindrical coordinate system for the neck with z representing the axial coordinate, r the radial coordinate, and z_1 and z_2 the end points of the neck on the axial coordinate, as shown in Fig. 2. Then, a series of parameters are defined based on the coordinate system: r_0 represents minimum radius of curvature along the radial orientation of the neck and r_c the axial one, V_N the volume of the gaseous neck enclosed by the interface between z_1 and z_2, Q_N the gradient of V_N with time, p the capillary pressure at the minimum radius and the values of the parameters could be directly obtained from Eqs. (1)–(5), respectively. It is noticeable that the positive p promotes the collapse of the neck.

$$r_0 = f(0) \tag{1}$$

$$r_c = \frac{\{1+[f'(0)]^2\}^{3/2}}{f''(0)} \tag{2}$$

$$V_N = \int_{z_1}^{z_2} \pi[f(z)]^2 dz \tag{3}$$

$$Q_N = -dV_N/dt \tag{4}$$

$$p = \sigma(1/r_0 - 1/r_c) \tag{5}$$

The evolution of the minimum radius of the neck with the remaining time for a series of liquid flow rates is illustrated in Fig. 3a. The neck collapses acceleratingly with the remaining time, for a fixed liquid flow rate. At the beginning of the collapse, the effect of the liquid flow rate on the collapse is remarkable: the initial shrinking rate enlarges rapidly with the increase in the liquid flow rate. And then, the effect of the liquid squeezing weakens with the
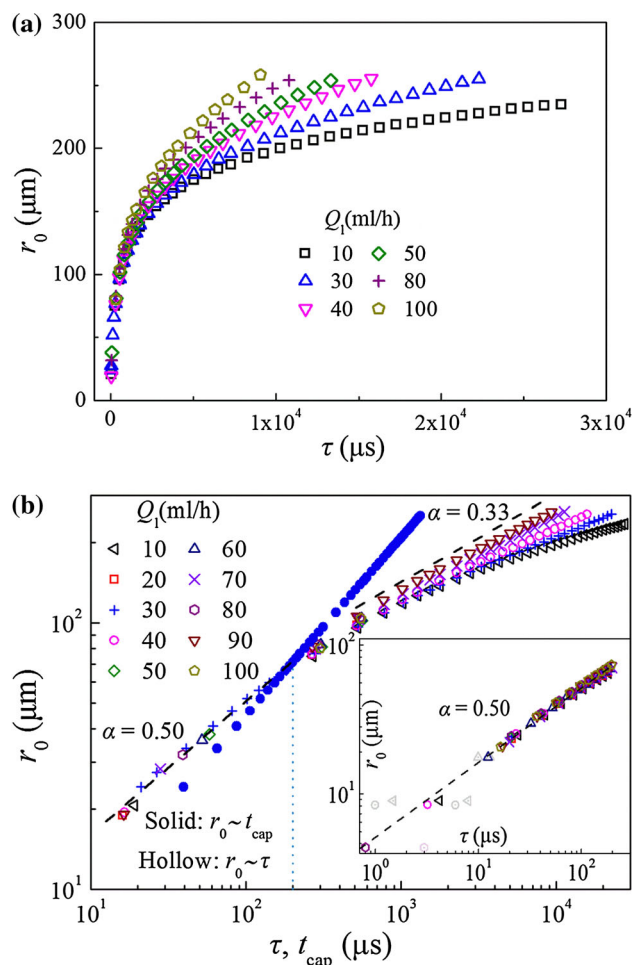

Fig. 3 **a** The evolution of the minimum radius of the gaseous neck r_0 with remaining time until the pinch-off (τ) under a series of liquid flow rates. $\tau = t_c - t$, t the collapse time and t_c the time for the final breakup of the neck. **b** The minimum radius r_0 as a function of the remaining time τ and the local capillary time (t_{cap}) in a logarithmic coordinate system. t_{cap} represents the value of local capillary time for the condition of $Q_l = Q_g = 30$ mL h^{-1}. The *dashed lines* with various slopes are used to define the exponent. The *dotted line* marks the time of $t_{cap} = \tau$. The *inset* figure illustrates the collapsing exponent for the free pinch-off stage referring to the *dashed line*. The *lighter dot centered symbols* indicate the maximum deflection resulted from the error in estimating the moment of breakup. $Q_g = 30$ mL h^{-1}

remaining time, displayed as the concentrating curves for a series of liquid flow rates. After a sudden speedup of the collapse, the neck thins along a common trajectory, and the effect of the flow rate becomes negligible.

The pinch-off rules are estimated by assuming $r_0 = A\tau^\alpha$, referring to the method of Bergmann et al. (2009), and the value of α can be attained by the least-square fitting method as shown in Fig. 3b. It is shown that the collapse exponent experiences a sudden increase for each liquid flow rate. To distinguish the breakup stages with different rules, we bring in the local capillary time t_{cap} ($t_{cap} = \sqrt{\rho r_0^3/\sigma}$) as a
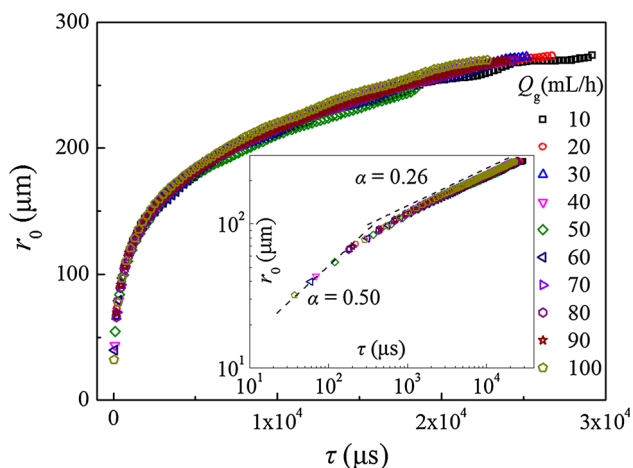
Fig. 4 The evolution of the minimum radius of the gaseous neck r_0 with the remaining time τ under a series of gas flow rates. The *inset* figure shows the collapsing exponents with referring to the *dashed lines*. $Q_l = 30$ mL h^{-1}

Fig. 5 Evolution of the slenderness λ with the remaining time τ. $Q_g = 30$ mL h^{-1}

criterion (van Hoeve et al. 2011). The capillary time is a timescale for the interface to recover its shape after a perturbation in inviscid liquid (Eggers 1997). If the thinning rate of the neck is much faster than the typical rate of the interface relaxation under capillary force, i.e., $t_{cap} > \tau$, the collapse process is free of the constriction of the liquid (Garstecki et al. 2005). We plot the evolution of the local capillary time with the remaining time in Fig. 3b and find that: t_{cap} is less than τ, before the sharp speedup; and t_{cap} is larger than τ, after the speedup. It is profound that all of the speedup occurs around the moment of $t_{cap} = \tau$. Therefore, we divide the nonlinear collapse process into two stages by the time criterion of t_{cap}. In the first stage ($t_{cap} < \tau$), the exponent increases with the increase in liquid flow rate and approaches to 0.33 eventually. Considering the key role of liquid squeezing, we call the process the liquid squeezing collapse stage. In the latter stage ($t_{cap} > \tau$), the neck shrinks at a universal exponent of 0.50 for a series of liquid flow rates as shown in Fig. 3b. As the report of Burton et al. (2005) and Thoroddsen et al. (2007), the universal exponent reveals the rule of self-similar process; therefore, we define this process as the free pinch-off stage. Contrast with the liquid flow rate, the gas flow rate has no obvious effect on the nonlinear collapse, as shown in Fig. 4.

Overall, the collapse dynamics for the Taylor bubble formation in a flow-focusing device is similar to that demonstrated by van Hoeve et al. (2011), but is different from the free-surface collapse process (Basaran 2002; Bird et al. 2010; Burton et al. 2005; Eggers 1997; Eggers and Villermaux 2008; González and García 2009; Thoroddsen et al. 2007). To our knowledge, the transition of the exponent in the conventional process has not been reported and the significant role of the liquid flow rate during the collapse process is revealed for the first time. And the
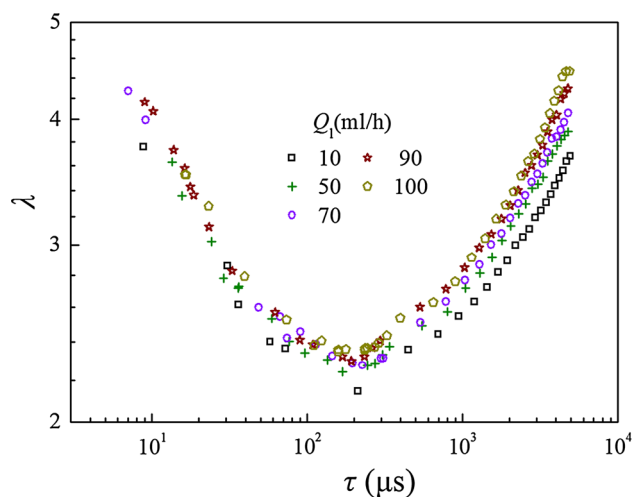
concurrence of the enlarging exponent and the fading liquid constriction implies the distinct effect of liquid squeezing on the transition of the exponent. These results arouse our curiosity to explore the breakup mechanism for Taylor bubble formation.

3.2 Breakup mechanism for Taylor bubble formation

3.2.1 The transition of the exponential scale

Capillary force plays a key role during the bubble pinch-off (Eggers et al. 2007), and its value consists of the radial and axial components for the axisymmetric neck. Therefore, the shape of the gaseous neck is an important parameter to characterize the variations of exponents (Eggers et al. 2007; Gekle et al. 2009). Here, we defined the slenderness λ as the ratio of the axial radius of curvature to the radial one of the gaseous neck ($\lambda = r_c/r_0$), as done in van Hoeve et al. (2011). The larger the slenderness is, the more slender is the gaseous neck. The temporal evolution of the slenderness of the gaseous neck is plotted in Fig. 5. It is shown that λ exceeds 2 during the nonlinear collapse in all of the conditions. Therefore, p is always larger than zero referring to Eq. 5, indicating that the surface tension drives the whole nonlinear collapse process.

In the liquid squeezing collapse stage, λ decreases with time and increases with the increase in the liquid flow rate. But during the free pinch-off stage, the slenderness of the neck increases with time in the same way regardless of the liquid flow rate. The evolution of the slenderness illustrates that liquid constriction plays a key role on the liquid squeezing collapse stage during the bubble formation process, and the gaseous thread collapses under an identical dominating effect in the free pinch-off stage. These

tendencies also imply that there is a fierce interface rearrangement accompanying with the transition of exponent, and the transition of exponent is the result of the interface rearrangement. The phenomenon of the interface arrangement for bubbles formation in a T-junction device was also implied (van Steijn et al. 2009): a convex surface evolved to a concave shape just at the beginning of the sudden accelerating collapse.

It is noteworthy that the temporal evolution of the slenderness in our work is incompatible with the reported works (Eggers et al. 2007; van Hoeve et al. 2011). In the liquid squeezing collapse stage, the axial length scale decreases faster than the radial one. This tendency is contrary to the characteristic of the conventional free-surface pinch-off process (Eggers et al. 2007; Thoroddsen et al. 2007). This inconformity can be attributed to the constriction of the liquid with constant flow rate in the flow-focusing region during the collapse. For the free pinch-off stage, the radial length shrinks more rapidly than the axial one, resulting in a more and more slender neck. This tendency is consistent with the free-surface collapse (Eggers et al. 2007; Thoroddsen et al. 2007), but contrary to the conclusion of van Hoeve et al. (2011). In the experiment of van Hoeve et al. (2011), the neck becomes less and less slender, which is similar to the rule of the liquid squeezing collapse stage. This divergence may be caused by the different flow regimes. In the report of van Hoeve et al. (2011), the bubble was formed without touching the walls of the channel and the unconfined spherical gaseous tip might keep off the rearrangement of the neck. However, in our experiment, the slender neck thins in the broad flow-focusing region, and the gaseous thread is restricted completely by the main channel.

3.2.2 The driving forces during nonlinear collapse

During the free pinch-off stage, the relative importance of inertial forces, viscous forces and surface tension forces can be characterized by the instantaneous Reynolds number and Weber number (Gekle et al. 2009; Thoroddsen et al. 2007; van Hoeve et al. 2011). The relative importance of inertial forces to viscous forces is given by the Reynolds number

$$Re = \frac{\rho_l r_0 r_0'}{\eta_l} \tag{6}$$

The Weber number characterizing the relative importance of inertial forces to surface tension forces is expressed as

$$We = \frac{\rho r_0 (r_0')^2}{\sigma} \tag{7}$$

Based on the experimental data, we plot both Re and We versus the remaining time until the pinch-off in Fig. 6. It is
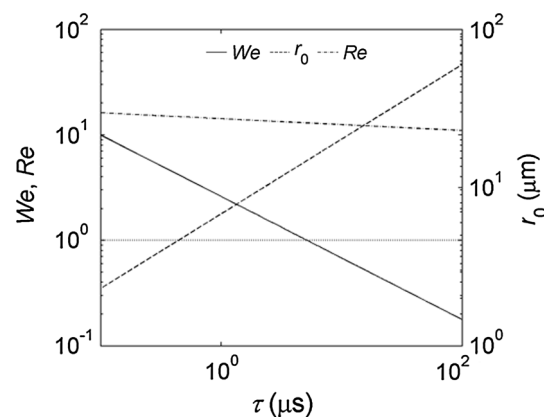

Fig. 6 Temporal evolution of Weber number We, Reynolds number Re and radial radius of curvature r_0 as a function of the remaining time τ during the free pinch-off stage. The *horizontal dotted line* gives the value of unity for Weber number and Reynolds number. $Q_l = Q_g = 30$ mL h^{-1}

shown that the Reynolds number is much greater than unity during the entire collapse process, suggesting that inertial forces play more important role than viscous forces. The We is less than one initially, but larger than one approaching the singularity at pinch-off. Hence, the process is initiated by the interfacial tension and the gaseous thread finally breaks up mainly dominated by liquid inertia. The sustained dominating role of inertia force near breakup further identifies that the universal exponent of 0.5 observed in the free pinch-off stage reveals the rule of self-similar process for the pinch-off of bubbles (Eggers et al. 2007).

3.2.3 Role of the liquid squeezing under the confinement

During the nonlinear collapse, the leakage through the gutters between the wall of the channel and the gaseous thread is weak (van Steijn et al. 2009). Therefore, the role of liquid constriction can be estimated by analyzing relative importance of liquid flow rate Q_l and gradient of the volume of with the remaining time Q_N. When the neck collapses slowly ($Q_N < Q_l$), the original nonlinear breakup process is constricted by the liquid phase (Garstecki et al. 2005). However, if the neck collapses so rapidly that Q_N is larger than Q_l, the liquid restriction on the gaseous thread is terminated, which results in a reverse flow through the gutter from the tip to the neck of the gaseous thread (van Steijn et al. 2009). The evolution of the gradient of the neck volume Q_N is plotted in Fig. 7. And throughout almost the entirety of the squeezing collapse stage, Q_N is less than Q_l. It indicates that the neck collapses under the liquid restriction, which can interpret the increase in the exponent and the slenderness with the increase in the liquid flow rate. However, in the whole free breakup stage, Q_N is
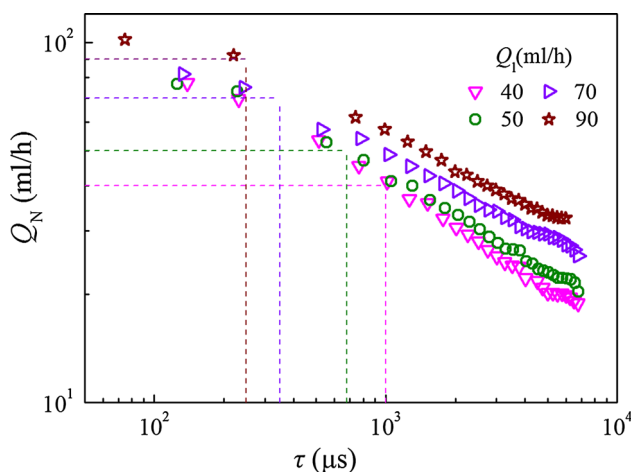
Fig. 7 Temporal evolution of the gradient of neck volume Q_N under a series of liquid flow rates. $Q_g = 30$ mL h^{-1}. The *dashed lines* mark the moments of $Q_N = Q_l$

always larger than Q_l. It demonstrates that the neck collapses without the effect of the liquid squeezing.

Figure 7 also indicates that interface rearrangement occurs accompanying with the reverse flow, and the reverse flow comes earlier for a lower liquid flow rate. This phenomenon demonstrates that the reverse flow is caused by the fading of the liquid constriction, triggering the interface rearrangement. Our result is incompatible with the report of van Steijn et al. (2009). van Steijn et al. (2009) observed the reverse flow originally in a T-junction and proposed that the reverse flow was the result of the pressure gradient between the thread tip and the neck. Consequently, the liquid reversed at a fixed r_0 in a straight channel. The deviation may be resulted from the variation of the neck's shape under different liquid flow rates as discussed in the section of 3.2.1.

3.2.4 Theory analysis of the collapse regulation

The slenderness λ increases sharply approaching to the pinch-off, according to Fig. 5. Together with the negligible liquid constriction, the free pinch-off process can be described by the cylindrical version of general Rayleigh–Plesset equation proposed by Plesset (1977) and Oguz and Prosperetti (1993):

$$\frac{P(R) - P_B}{\rho_L} = (r_0'' r_0 + (r_0')^2) \ln \frac{r_0}{R} + \frac{1}{2}(r_0')^2 - \frac{2\eta_L r_0' + \sigma}{\rho_L r_0} \tag{8}$$

where R is half of the channel width, ρ_L and η_L are the density and viscosity of the liquid, and $P(R)$ and P_B are the pressure near the channel wall and in the bubble. Resembling to Burton et al. (2005), we obtain a value of 0.5 for α by neglecting the axial motion (the collapsing rate of the gaseous neck is much greater than its axial moving rate in the

free pinch-off stage). But some larger exponents were also achieved ranging from 0.52 to 0.58 (Burton et al. 2004; Eggers et al. 2007; Thoroddsen et al. 2007) and the little increment was attributed to the unstable cylindrical solution (Eggers and Villermaux 2008). In our experiment, the confinement of the wall is identified to stabilize the gaseous thread (Dollet et al. 2008); therefore, the exponent should maintain the scale of 0.5 approaching to the pinch-off. In fact, Eggers et al. (2007) and Gekle et al. (2009) confirmed the scale approximated to 0.5 even in a timescale of nanosecond. In addition, the theoretical exponent of 0.5 is less than 0.64 ± 0.07 for the pinch-off of droplet formation in a similar device with the present experiments (Fu et al. 2012a, b) and 1 for the breakup of droplets in a T-junction (Hoang et al. 2013). The divergence may be caused by the marked difference of the density of the dispersed phase: the density ratio for the dispersed phases between the references (Fu et al. 2012a, b; Hoang et al. 2013) and the present experiment is about 10^3. The distinction of density among the dispersed phases results in the great disparity of inertia force near the pinch-off, which further leads to the obvious divergence of exponents between the two fluid systems according to the theoretical analysis of Eggers and Villermaux (2008).

It is noteworthy that, according to the report of Eggers et al. (2007) and Gekle et al. (2009), when $\tau \to 0$, $\alpha \to 0.5^+$, but $\alpha \to 0.5^-$ in our experiment. The divergence can be attributed to the different flow conditions during the formation of bubbles. In our experiment, the neck collapses originally under the constriction of liquid with an exponent <0.33. But for the breakup of gaseous thread in conventional case (Eggers et al. 2007; Gekle et al. 2009), the collapse starts under the domination of surface tension, leading to an exponent about 0.6 (Eggers et al. 2007). Nevertheless, the final collapse process always follows the singularity independent of the liquid constriction as: $\tau \to 0$, $\alpha \to 0.5$.

Furthermore, the range of the exponent scales for the squeezing collapse stage can be predicted according to volume conservation. Under the constriction of the liquid, the evolution of the interface in flow-focusing region mainly occurs around the neck (Gekle et al. 2009). Therefore, the gradient of the neck's volume Q_N is approximately equal to the liquid flow rate Q_l:

$$Q_N \approx -r_0 r_c r_0' = Q_l \tag{9}$$

$$-r_0 r_c r_0' = \text{const} \tag{10}$$

The r_c is assumed to follow a power–law relation with the remaining time as $r_c \propto \tau^\beta$ (van Hoeve et al. 2011), and then,

$$\tau^{2\alpha + \beta - 1} = \text{const} \tag{11}$$

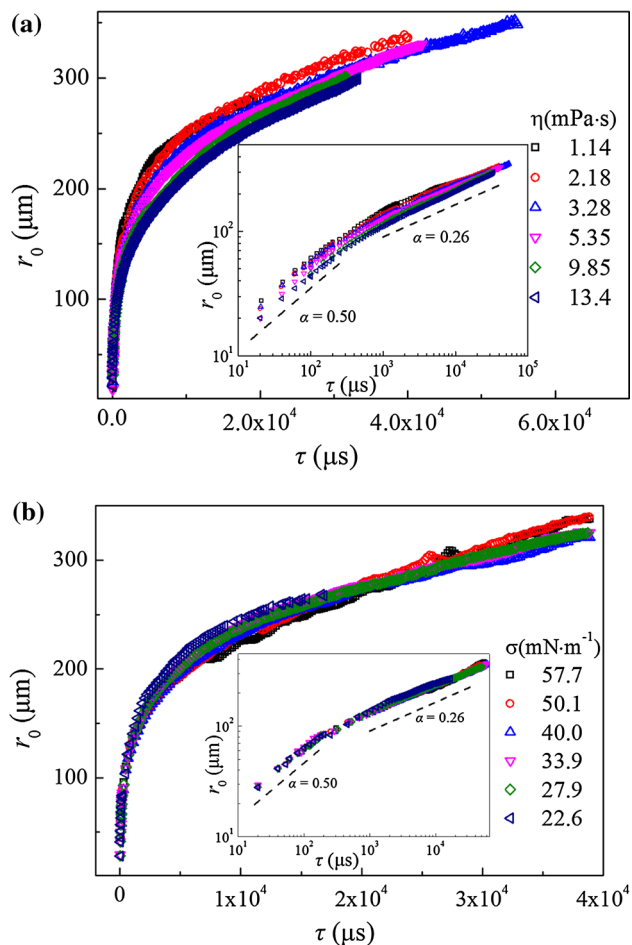In the liquid squeezing collapse stage, the neck becomes less slender with time, and $\alpha > \beta$ (Fig. 5). Thus, α is less

(a)

(b)

Fig. 8 The evolution of the minimum radius of the gaseous neck r_0 with the remaining time τ: **a** under a series of liquid viscosities; **b** under a series of surface tensions. The *inset* figures show the collapsing exponents with referring to the *dashed lines*. $Q_l = Q_g = 30$ mL h^{-1}

than 0.33 according to Eq. 11. Therefore, as the increase in the liquid flow rate, the value of α approaches to 0.33, as displayed in Fig. 3b.

3.3 Validating of the breakup mechanism

The effects of physical properties of liquid phase on the interface breakup process were obvious as shown in the works of Burton et al. (2005) and Thoroddsen et al. (2007). Therefore, the influences of the liquid viscosity and surface tension on the nonlinear breakup during bubble formation are further investigated. As shown in Fig. 8a, the scale remains 0.5 in free pinch-off stage and 0.26 in liquid squeezing stage, though the collapse velocity decreases slightly as the increase in liquid viscosity. It is demonstrated that the viscous force has weak influence on the bubble pinch-off process under low liquid viscosity. The

phenomenon can be attributed to the minor role of viscous stress during the breakup and is consistent with the work of Burton et al. (2005) and Thoroddsen et al. (2007). Resemble to the slight influence of liquid viscosity, the surface tension has also no obvious effect on the nonlinear collapse, as shown in Fig. 8b. The negligible influence of the surface tension can be attributed to the driving role of the surface tension during the breakup (Eggers et al. 2007). It is identified that nonlinear breakup mechanism is valid under low liquid viscosities (1–13.4 m Pa s) and various surface tensions (23–57 m N m^{-1}) with the capillary number Ca for the continuous phase ranges from 0.0004 to 0.0045.

4 Conclusions

This work investigates the pinch-off mechanism for Taylor bubble formation in a microfluidic flow-focusing device. And the results show that the gaseous neck collapses nonlinearly with time and the minimum width of the gaseous thread r_0 can be scaled with the remaining time τ as a power–law relationship: $r_0 \propto \tau^\alpha$. Two distinct collapse processes are observed: the liquid squeezing collapse stage and the free pinch-off stage. In the liquid squeezing collapse stage, the collapse is induced by the liquid constriction. The exponent α increases with the increase in the liquid flow rate and approaches to 0.33 eventually. While in the free pinch-off stage, the value of α is close to 0.5 and is independent of the liquid flow rate. The transition of the exponent between the two stages is triggered by the interface rearrangement resulted from the reversal of the liquid due to the fading of liquid constriction. The analyses of the governing forces exerted on the gaseous thread during the bubble formation process show that the final pinch-off is dominated by the liquid inertia, and the surface tension is still important. The mechanism is identified to be valid under low liquid viscosities (1–13.4 m Pa s) and various surface tensions (23–57 m N m^{-1}) with the capillary number Ca ranges from 0.0004 to 0.0045. The refined stages can be further used to predict the frequency and volume for the generation of bubbles and the relevant work is in process (Dang et al. 2013; Fu et al. 2009). Our study of nonlinear breakup dynamics for bubble formation under confinement is helpful for further theoretical and experimental investigations on the regulation of bubbles in microfluidics and the design of microfluidic devices.

References

Abadie T, Aubin J, Legendre D, Xuereb C (2012) Hydrodynamics of gas–liquid Taylor flow in rectangular microchannels. Microfluid Nanofluid 12:355–369

Basaran OA (2002) Small-scale free surface flows with breakup: drop formation and emerging applications. AIChE J 48:1842–1848

Bergmann R, van der Meer D, Gekle S, van der Bos A, Lohse D (2009) Controlled impact of a disk on a water surface: cavity dynamics. J Fluid Mech 633:381–409

Bird JC, de Ruiter R, Courbin L, Stone HA (2010) Daughter bubble cascades produced by folding of ruptured thin films. Nature 465:759–762

Burton JC, Rutledge JE, Taborek P (2004) Fluid pinch-off dynamics at nanometer length scales. Phys Rev Lett 92:244505

Burton JC, Waldrep R, Taborek P (2005) Scaling and instabilities in bubble pinch-off. Phys Rev Lett 94:184502

Dang M, Yue J, Chen G, Yuan Q (2013) Formation characteristics of Taylor bubbles in a microchannel with a converging shape mixing junction. Chem Eng J 223:99–109

Dollet B, van Hoeve W, Raven JP, Marmottant P, Versluis M (2008) Role of the channel geometry on the bubble pinch-off in flow-focusing devices. Phys Rev Lett 100:034504

Eggers J (1997) Nonlinear dynamics and breakup of free-surface flows. Rev Mod Phys 69:865–930

Eggers J, Villermaux E (2008) Physics of liquid jets. Rep Prog Phys 71:036601

Eggers J, Fontelos MA, Leppinen D, Snoeijer JH (2007) Theory of the collapsing axisymmetric cavity. Phys Rev Lett 98:094502

Ferrara KW, Borden MA, Zhang H (2009) Lipid-shelled vehicles: engineering for ultrasound molecular imaging and drug delivery. Acc Chem Res 42:881–892

Fu T, Ma Y, Funfschilling D, Li HZ (2009) Bubble formation and breakup mechanism in a microfluidic flow-focusing device. Chem Eng Sci 64:2392–2400

Fu T, Funfschilling D, Ma Y, Li HZ (2010) Scaling the formation of slug bubbles in microfluidic flow-focusing devices. Microfluid Nanofluid 8:467–475

Fu T, Ma Y, Funfschilling D, Zhu C, Li HZ (2012a) Breakup dynamics of slender bubbles in non-newtonian fluids in microfluidic flow-focusing devices. AIChE J 58:3560–3567

Fu T, Wu Y, Ma Y, Li HZ (2012b) Droplet formation and breakup dynamics in microfluidic flow-focusing devices: from dripping to jetting. Chem Eng Sci 84:207–217

Ganan-Calvo AM, Gordillo JM (2001) Perfectly monodisperse micro-bubbling by capillary flow focusing. Phys Rev Lett 87:274501

Garstecki P, Gitlin I, DiLuzio W, Whitesides GM, Kumacheva E, Stone HA (2004) Formation of monodisperse bubbles in a microfluidic flow-focusing device. Appl Phys Lett 85:2649–2651

Garstecki P, Stone HA, Whitesides GM (2005) Mechanism for flow-rate controlled breakup in confined geometries: a route to monodisperse emulsions. Phys Rev Lett 94:164501

Gekle S, Snoeijer JH, Lohse D, van der Meer D (2009) Approach to universality in axisymmetric bubble pinch-off. Phys Rev E 80:036305

González H, García FJ (2009) The measurement of growth rates in capillary jets. J Fluid Mech 619:179–212

Hartman RL, Naber JR, Buchwald SL, Jensen KF (2010) Multistep microchemical synthesis enabled by microfluidic distillation. Angew Chem Int Ed 49:899–903

Hoang DA, Portela LM, Kleijn CR, Kreutzer MT, van Steijn V (2013) Dynamics of droplet breakup in a T-junction. J Fluid Mech 717:R4

Kashid MN, Renken A, Kiwi-Minsker L (2011) Gas–liquid and liquid–liquid mass transfer in microstructured reactors. Chem Eng Sci 66:3876–3897

Kreutzer MT, Kapteijn F, Moulijn JA, Kleijn CR, Heiszwolf JJ (2005) Inertial and interfacial effects on pressure drop of Taylor flow in capillaries. AIChE J 51:2428–2440

Li W, Liu K, Simms R, Greener J, Jagadeesan D, Pinto S, Günther A, Kumacheva E (2011) Microfluidic study of fast gas–liquid reactions. J Am Chem Soc 134:3127–3132

Nghe P, Terriac E, Schneider M, Li ZZ, Cloitre M, Abecassis B, Tabeling P (2011) Microfluidics and complex fluids. Lab Chip 11:788–794

Oguz HN, Prosperetti A (1993) Dynamics of bubble growth and detachment from a needle. J Fluid Mech 257:111–145

Plesset MS (1977) Bubble dynamics and cavitation. Ann Rev Fluid Mech 9:145–185

Sun R, Cubaud T (2011) Dissolution of carbon dioxide bubbles and microfluidic multiphase flows. Lab Chip 11:2924–2928

Tadmor AD, Ottesen EA, Leadbetter JR, Phillips R (2011) Probing individual environmental bacteria for viruses by using microfluidic digital PCR. Science 333:58–62

Thoroddsen ST, Etoh TG, Takehara K (2007) Experiments on bubble pinch-off. Phys Fluids 19:042101

Tumarkin E, Nie Z, Park JI, Abolhasani M, Greener J, Sherwood-Lollar B, Gunther A, Kumacheva E (2011) Temperature-controlled 'breathing' of carbon dioxide bubbles. Lab Chip 11:3545–3550

Utada AS, Lorenceau E, Link DR, Kaplan PD, Stone HA, Weitz DA (2005) Monodisperse double emulsions generated from a microcapillary device. Science 308:537–541

van Hoeve W, Dollet B, Versluis M, Lohse D (2011) Microbubble formation and pinch-off scaling exponent in flow-focusing devices. Phys Fluids 23:092001

van Steijn V, Kleijn CR, Kreutzer MT (2009) Flows around confined bubbles and their importance in triggering pinch-off. Phys Rev Lett 103:214501

Wang K, Lu Y, Tan J, Yang B, Luo G (2010) Generating gas/liquid/liquid three-phase microdispersed systems in double T-junctions microfluidic device. Microfluid Nanofluid 8:813–821

Wörner M (2012) Numerical modeling of multiphase flows in microfluidics and micro process engineering: a review of methods and applications. Microfluid Nanofluid 12:841–886

Zhao Y, Chen G, Yuan Q (2007) Liquid–liquid two-phase mass transfer in the T-junction microchannels. AIChE J 53:3042–3053